Three-Dimensional Mode Conversion Associated with Kinetic Alfvén Waves

Yu Lin, Jay R. Johnson, and Xueyi Wang

Phys. Rev. Lett. **109**, 125003 — Published 20 September 2012

DOI: 10.1103/PhysRevLett.109.125003

Three-Dimensional Mode Conversion Associated with Kinetic Alfvén Waves

Yu Lin

*Physics Department, Auburn University, Auburn, AL 36849-5311, USA**

Jay R. Johnson

Princeton Plasma Physics Laboratory, Princeton, NJ 08543, USA

Xueyi Wang

Physics Department, Auburn University, Auburn, AL 36849-5311, USA

Abstract

We report the first three-dimensional (3-D) ion particle simulation of mode conversion from a fast mode compressional wave to kinetic Alfvén waves (KAWs) that occurs when a compressional mode propagates across a plasma boundary into a region of increasing Alfvén velocity. The magnetic field is oriented in the $\hat{z}$ direction perpendicular to the gradients in the background density and magnetic field ($\hat{x}$). Following a stage dominated by linear physics in which KAWs with large wave numbers $k_x\rho_i \sim 1$ (with ρ_i being the ion Larmor radius) are generated near the Alfvén resonance surface, the growth of KAW modes with $k_y\rho_i \sim 1$ is observed in the nonlinear stage when the amplitude of KAWs generated by linear mode conversion becomes large enough to drive a nonlinear parametric decay process. The simulation provides a comprehensive picture of mode conversion and the fundamental importance of the 3-D nonlinear physics to transfer energy to large perpendicular k_y modes, which can provide large transport across plasma boundaries in space and laboratory plasmas.

PACS numbers: 52.35.Mw, 94.05.Pt, 94.30.ch, 52.65.-y, 94.30.cq

INTRODUCTION

Mass, momentum, and energy transport at plasma boundaries is of fundamental importance to the dynamics and stability of space and laboratory plasma physics. Wave-particle interactions provide an effective means to facilitate such transport, and they are most effective when the fluctuations are on kinetic scales. Moreover, inhomogeneities in the plasma density and magnetic fields at these boundaries allow for coupling and mode conversion from global scale MHD modes to kinetic scale waves [1]. The Earth's magnetopause boundary provides an example of a region where it is believed that wave-particle diffusive processes are important [2–7], particularly for periods of northward interplanetary magnetic field when massive cross-field line plasma entry occurs. It has been suggested theoretically that mode conversion from incident compressional waves to kinetic Alfvén waves (KAWs) at the magnetopause leads to the plasma transport [4]. KAWs are low frequency ($\omega < \Omega_i$) waves with kinetic scale $k_\perp \rho_i \sim 1$ spatial variation, where Ω_i is the ion gyrofrequency, ρ_i is the ion Larmor radius, and $k_\perp$ is the perpendicular wave numbers. Recent THEMIS spacecraft observations [7] show a direct evidence of a turbulent spectrum of KAWs at the magnetopause with sufficient power to provide massive particle transport, $D_\perp \sim 10^{9-10} m^2/s$. A similar mode conversion process may also occur on closed field lines in the magnetosphere to drive field-line resonances that have been associated with auroral precipitation [8]. KAWs generated in the solar wind and corona through mode conversion [9] or nonlinear cascade may also play an important role in particle heating [10] and powering the fast solar wind [11]. Additionally, KAWs play crucial roles in magnetic fusion devices [12]. Laboratory plasma experiments have shown evidence of coupling between toroidal Alfven eigenmodes (TAEs) and KAWs [13] that may also be externally driven by mode conversion of fast modes [14]. Although important in a variety of space and laboratory contexts, the nonlinear physics of mode conversion of the KAW remains poorly understood.

In this letter, we report the first ion kinetic simulation of three-dimensional (3-D) nonlinear physics of mode conversion from a fast-mode compressional wave to kinetic Alfvén waves (KAWs) that occurs when a large amplitude compressional mode propagates across a plasma boundary into an increasing Alfvén velocity. The parameters that we select for these simulations are relevant for the Earth's magnetopause, where fast-mode waves that originate from either solar wind compressions or from the foreshock [15] propagate against

the magnetopause. In the simulation, the initial magnetic field points along $\hat{z}$, perpendicular to the boundary nonuniformity ($\hat{x}$). It is shown that KAWs with a large wave number $k_y\rho_i \sim 1$ that is perpendicular to both the background magnetic field $\mathbf{B}_0$ and the wave vector $\mathbf{k}_0$ of the incident fast-mode wave are nonlinearly excited in the mode conversion process. Because transport is proportional to k_y^2 [2, 4, 5], the nonlinear excitation of these modes resulting from dynamics in the $\hat{y}$ direction as shown in this paper is critical to understanding transport.

SIMULATION DETAILS

The magnetopause boundary is modeled with a slab geometry with total pressure balance, separating uniform regions of the magnetosheath and magnetosphere. For comparison, the initial setup and parameters are the same as those used in the 2-D (xz only) simulations of Lin et al. [16]. The magnetosheath ion beta $\beta_{is} = 0.5$, corresponding to $\rho_{is} = 0.5d_{is}$, where ρ_{is} and d_{is} are the ion Larmor radius and ion skin depth in the magnetosheath, respectively. The electron-to-ion temperature ratio is assumed to be $T_{e0}/T_{i0} = 0.4$. The half-width of the magnetopause boundary layer is assumed as $D_0 = 7.5d_{is}$. The ratio between the magnetosheath and magnetospheric ion density is $N_s/N_m = 10$. The Alfvén speed V_A increases by nearly a factor of 4 through the magnetopause boundary. The incident sinusoidal compressional wave is imposed from the boundary ($x = 0$) in the magnetosheath with frequency $\omega_0 = 0.4$ and wave number, $(k_{x0}, k_{y0}, k_{z0}) = (0.262, 0, 0.196)$ in the xz plane, corresponding to $\omega_0/(k_{\|0}V_{As}) = 2.0$, where the subscript "$\|$" indicates the direction parallel to $\mathbf{B}_0$. The amplitude in the flow speed of the incident wave is $\delta V_i = 0.2V_{As}$.

A hybrid simulation model is used, in which ions are treated as fully kinetic particles moving in a self-consistent electromagnetic field, and electrons are treated as a corresponding massless fluid. A 3-D simulation grid with dimensions $n_x \times n_y \times n_z = 200 \times 65 \times 65$ is used with uniform grid sizes $\Delta x = 0.5d_{is}$, $\Delta y = d_{is}$, and $\Delta z = 2d_{is}$. Free boundary conditions are used at $x = 100$ on the magnetospheric side. Periodic boundary conditions are assumed at all the other four boundary surfaces. In the presentation below, the time is normalized to Ω_s^{-1}, where Ω_s is the ion gyrofrequency in the magnetosheath. The magnetic field is expressed in units of the magnetosheath field B_s, and the ion number density in units of the magnetosheath density N_s. The velocity is normalized to the magnetosheath Alfvén speed

V_{As}, and the spatial coordinates are normalized to d_{is}.

SIMULATION RESULTS

Figure 1 shows the simulation results at $t = 200$ in the xz and xy planes. For reference, the magnetopause boundary is located at $42.5 < x < 57.5$ separating the magnetosheath $x < 42.5$ and magnetosphere $x > 57.5$. The Alfvén resonance condition $\omega^2 = k_\parallel^2 V_A^2 (1-\omega^2/\Omega_i^2)^2$[1] is satisfied at $x \simeq 53$, which is the predicted mode conversion point according to linear kinetic theory [3, 4, 17–22]. The top row of Figure 1 depicts the resulting contours of ion density N, magnetic field components B_x and B_y, electric fields E_x and E_y, and the parallel electric field $E_\parallel$ in the xz plane around the magnetopause at $y = 32$ and $t = 200$. Larger-amplitude, short wavelength waves are excited in the transition layer between $x \simeq$ 47-60 around the Alfvén resonance point, in addition to the incident and reflected compressional waves on the magnetosheath side dominated by perturbations in B_x, E_y and N. Similar to the 2-D results for the same case[16], these waves show characteristics of KAWs with large and broadband wave vectors, $k_x\rho_i \sim 1$, dominated by perturbations in B_y, E_x, $E_\parallel$, and parallel current density $J_\parallel$ (not shown). These short wavelength waves radiate back to the magnetosheath.

The bottom row of Figure 1 shows the corresponding results in the yz plane tangential to the magnetopause, at the resonant point $x = 53$. Strong wave perturbations with finite wavelengths along y have clearly formed, while $k_y = 0$ in the incident wave. Spectral analysis of the power of B_x in the k_y-$k_\parallel$ plane is shown in Figure 2 for the wave structures at $x = 53$. Similar to the 2-D results [16], power peaks at discrete $k_{\parallel 0}$'s are present along $k_y = 0$, corresponding to multiple harmonics of the driving frequency, ω_0. An obvious 3-D effect is the presence of wave powers at large $k_y \sim 1$, corresponding to $k_y\rho_{is} \sim 0.5$ again with harmonics of $k_{\parallel 0}$. Meanwhile, harmonics of the nonlinearly excited $k_y \sim 1$ are also present.

The left column of Figure 3 shows the time evolution of powers of B_x (black), B_y (green), E_y (blue), and $E_\parallel$ (red) of the modes dominated by k_x, with $(k_x, k_z) = (-1.0, 0.196)$ and all k_y obtained in the plane at $y = 32$. B_y and $E_\parallel$ are seen to grow from $t = 40$, when the incident fast wave reaches the magnetopause boundary, while B_x and E_y show no growth as expected for KAWs dominated by k_x. This first-stage growth of KAWs from $t =$ 40-80 is due to the linear physics of mode conversion from the fast wave to KAWs. The powers are saturated at $t \sim 80$.

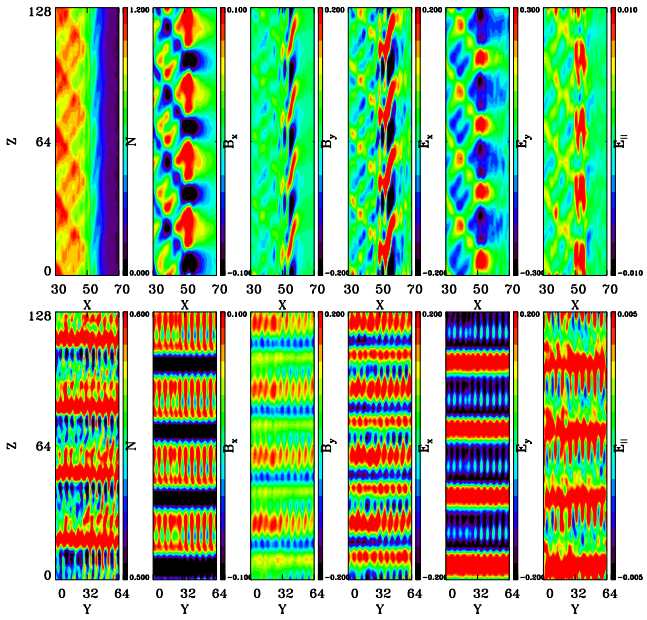

FIG. 1. Contours of various quantities at $t = 200$ in the xz plane (top row) at $y = 32$ and the yz plane (bottom row) at the Alfvén resonant point $x = 53$ obtained from the simulation of mode conversion in the inhomogeneous magnetopause.

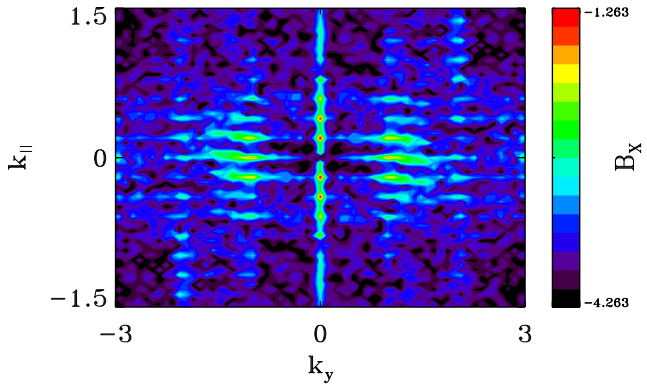

FIG. 2. k_y-$k_{||}$ spectra of B_x structures in the bottom row of Figure 1.

The mode coupling to k_y takes place in $t > 80$, in which the nonlinear physics plays a significant role, as illustrated in the right column of Figure 3 for the dominant k_y modes with $(k_y, k_z) = (-1.0, 0.196)$ and all k_x at the resonance point $x = 53$. In the second stage, from $t = 80$-145, the strong growth in B_x, E_y, and $E_{||}$ is consistent with KAWs dominated by k_y, which nonlinearly co-exist with the KAWs dominated by k_x. Finally for $t > 145$, the wave perturbations grow in all components. The mechanism for this final isotropic growth is beyond the scope of this paper.

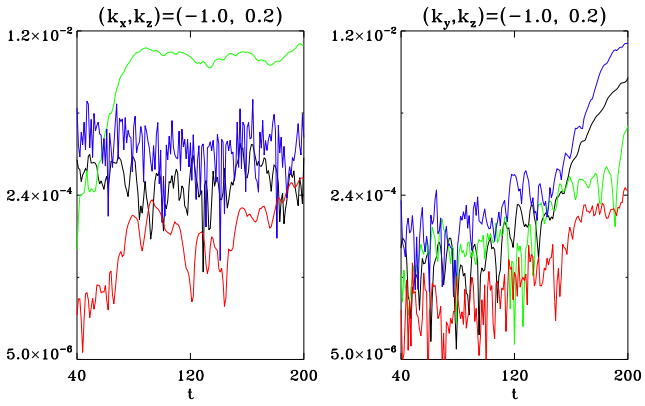

FIG. 3. Time evolution of B_x (black), B_y (green), E_y (blue), and $E_\parallel$ (red) for the KAW modes dominated by k_x (left column) at $y = 32$ and for those dominated by k_y (right) at the resonance point $x = 53$ in the inhomogeneous magnetopause.

The time evolution shown in Figure 3 suggests a nonlinear decay of the first-stage KAWs dominated by k_x to secondary KAWs dominated by k_y. The generation of the finite k_y spectrum for $t > 80$ results from nonlinear coupling in the kinetic equations that is ultimately linked with the $\mathbf{V}_E \cdot \nabla$ operator acting on perturbed fields, where $\mathbf{V}_E$ is the $\mathbf{E} \times \mathbf{B}$ velocity of the pump wave. In the linear stage the growing electric field of the KAW perturbations is dominated by the $\delta\mathbf{E}_x$ component so that $\mathbf{V}_E \simeq V_{Ey}\hat{y} \simeq \delta\mathbf{E}_x \times \mathbf{B}_{z0}$ which provides strong coupling to the k_y spectrum in the nonlinear stage.

Early theoretical work for cold ions [23, 24] and a recent extension to finite $k_\perp\rho_i$ [25] found that a pump KAW can nonlinearly decay into an ion acoustic mode and a lower-sideband daughter KAW through a parametric instability. For a pump KAW propagating with $\mathbf{k}_p = (k_{xp}, 0, k_{zp})$, the nonlinear coupling coefficient is proportional to $\Lambda = -i(c_s^2/2\Omega_i)(\mathbf{k}_s \times \mathbf{k}_p) \cdot \hat{z}$, where $\mathbf{k}_s = k_s\hat{y}$ is the wave vector of the ion acoustic mode. Since the pump mode has $k_{yp} = 0$, the wave number matching condition results in that the daughter KAW must have a finite wave number $\mathbf{k_d} = -k_s\hat{y}$. Nonlinear decay can also lead to ion heating through nonlinear ion Landau damping as seen in the simulation near the mode conversion region.

In order to examine the nonlinear decay of the first-stage KAWs, we show a supplemental hybrid simulation where we specify the driver wave and examine its decay in a homogeneous plasma. The inhomogeneity in the background plasma is not included in order to focus on the nonlinear stage. As in the inhomogenous simulation, we take $T_e/T_i = 0.4$, and $\beta_i = 0.5$ is assumed. The pump KAW is loaded at $t = 0$ with wave number $\mathbf{k}_p = (k_{xp}, 0, k_{zp}) =$

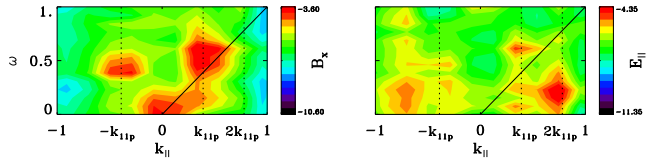

FIG. 4. $k_\parallel$-ω spectra of B_x and $E_\parallel$ obtained from the simulation of decay of an initial pump KAW in a uniform plasma. The solid black line indicates the dispersion relation of the MHD shear Alfvén mode for reference.

$(-1.6, 0, 0.196)$ and wave amplitude $\delta V_i = 0.6$. Higher spatial resolution ($\Delta x = 0.25$, $\Delta y = 0.5$, and $\Delta z = 0.5$) is used. To specify the single Fourier mode $\mathbf{k_p}$ of the pump wave, we filter out other modes from t = 0-10. But for $t > 10$, all modes in k_y and k_z are released, while only $k_x = 0$ and $|k_x| = k_{xp}$ are kept in k_x. The resulting real-space structures in the yz plane resemble those shown in the top row of Figure 1, with $k_y \gg k_z$.

These simplified simulations clearly demonstrate that a driven KAW nonlinearly decays into a daughter KAW and an ion acoustic wave, confirming the parametric decay process[23]. The $k_\parallel$-ω spectra of B_x and $E_\parallel$ shown in Figure 4 reveal the coupled modes. The initial pump KAW appears at $(k_{\parallel p}, \omega_p) = (0.2, 0.6)$ in $E_\parallel$, a daughter mode is present at $(k_{\parallel d}, \omega_d) = (-0.2, 0.4)$ in B_x and $E_\parallel$, and an ion sound wave is seen in $E_\parallel$ at $(k_{\parallel s}, \omega_s) = (0.4, 0.2)$. In addition, a low-frequency perturbation is also generated, around $(k_\parallel, \omega) \simeq (0, 0.05)$. Strong B_x perturbations are evident around the pump $(k_{\parallel p}, \omega_p)$.

The pump, daughter, and sound waves couple through a three-wave interaction because $\omega_p = \omega_d + \omega_s$ and $\mathbf{k}_p = \mathbf{k}_d + \mathbf{k}_s$. Since the system is symmetric in y, two dominant daughter waves are generated, with one at $k_{yd} > 0$ and the other at $k_{yd} < 0$, while their strengths are oscillating in time. The daughter KAWs have $k_{xd} = 0$ and $k_{yd} = \pm 1.2$, while the sound waves have $k_{xs} = k_{xp}$ and $k_{ys} = \mp 1.2$. The matching conditions are satisfied for each pair of the sound and daughter waves.

Figure 5 shows the time evolution of the powers of B_x and B_y in the pump wave $(k_{xp}, k_{yp}, k_{\parallel p}) = (1.6, 0, 0.2)$ and the pair of the daughter wave $(k_{xd}, k_{yd}, k_{\parallel d}) = (0, 1.2, -0.2)$ and sound wave $(k_{xs}, k_{ys}, k_{\parallel s}) = (1.6, -1.2, 0.4)$. As the pump wave (dominated by B_y) decays, the daughter wave (dominated by B_x) is excited and reaches a saturated level at $t \simeq 85$. The sound wave is a damped quasi-mode in the high beta plasma with $T_i > T_e$. It starts with nearly the same exponential growth rate as the daughter mode but then slows

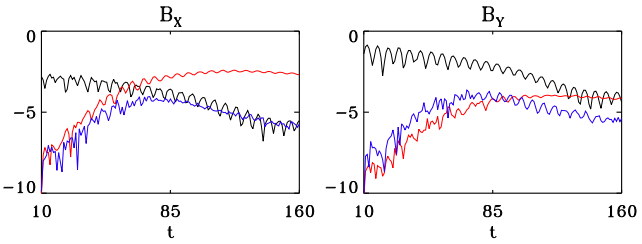

FIG. 5. Time evolution of B_x and B_y in the pump (black), daughter (red), and sound (blue) waves.

down and decays. The parametric growth rate can be estimated based on a three-wave interaction [23] by also including ion kinetic effects [25]. The growth rate of the daughter wave in the simulation obtained from analysis of the daughter wave spectrum is approximately $\gamma \sim 0.11\Omega_i$, very close to the theoretical growth rate of $\gamma \sim 0.14\Omega_i$ estimated from three-wave interactions including linear damping of the sound wave. The spectral analysis also exhibits further nonlinear coupling and energy flow to low frequency modes.

The additional low-frequency filamentary mode with $k_\parallel \simeq 0$ is found to have the strongest perturbations at the primary $k_x = 1.6$ and $k_y \simeq k_{yd} = 1.2$. This mode appears to be a zonal flow mode [26], or the convective cells [27]. The nonlinear excitation of zonal flows by Alfvénic turbulence or KAWs has been suggested by previous theoretical studies [26–28]. The nonlinear coupling of the zonal flow with the pump KAW leads to the B_x power with broadened spectral width around the pump frequency, as shown in the left plot of Figure 4. Zonal flows in fusion devices have also been studied with electrostatic simulations [29]. The zonal flows can break up the ion temperature gradient modes, leading to suppression of turbulent transport [29]. In our simulations the driver and daughter are electromagnetic; however, because the perpendicular wavelength is short, the modes are somewhat electrostatic in nature and the decay process may have some similarities.

The nonlinearly generated large k_y is important because it is crucial to the large transport across the boundary. The diffusion coefficient across a density gradient results from incoherent scattering from the perturbed velocity in the direction of the density gradient, including contributions from the perturbed $\mathbf{E} \times \mathbf{B}_0$ drift, the perturbed $\nabla \delta B$ drift (proportional to $\hat{b} \times \nabla \delta B_\parallel$, with $\hat{b} = \mathbf{B}_0/B_0$), and the field-aligned drift along the perturbed magnetic field ($v_\parallel \delta \hat{b} \sim v_\parallel \delta \mathbf{B}_\perp / B_0$). The component of these drifts across the magnetopause ($\hat{x}$) are all proportional to the azimuthal k_y, and the diffusion coefficient is proportional to k_y^2 [4, 5, 30]. The 3-D nonlinear effects are thus necessary to provide coupling to kinetic scales required

for efficient transport, and our simulations show clearly how mode conversion would lead to the development of a wave spectrum with $k_y\rho_i \sim 1$.Based on the observed wave spectrum at the magnetopause, massive transport ($D_\perp \sim 10^{9-10} m^2/s$) is expected [7].

SUMMARY

In summary, our simulation of mode conversion from a fast mode compressional wave to kinetic Alfvén waves in the nonuniform magnetopause boundary exhibits a multiple-stage process. First, KAWs are excited with large perpendicular $k_x\rho_i \sim 1$ in the nonuniformity direction near the Alfvén resonance surface due to the linear physics of mode conversion, which localizes the enhanced KAW wave energy. Then, KAW modes with large perpendicular and azimuthal wave numbers k_y are generated nonlinearly by parametric decay of the linearly generated primary KAWs. This parametric process is accompanied by the simultaneous excitation of zonal flow modes with similar large k_y. As such, the combination of the linear mode conversion and parametric decay leads to efficient transport at the plasma boundary. The 3-D nonlinear physics is crucial for understanding transport associated with the mode conversion. Our results show that mode conversion of compressional waves at the Alfvén velocity gradient quickly cascades to KAWs with large perpendicular and azimuthal wave number, which may lead to massive transport at the magnetopause and provide a mechanism of global plasma entry into the plasma sheet [4, 7]. The coupling of KAWs to the large-scale convective turbulence may play a significant role in the coupling between the ionosphere and magnetosphere [31], heating in the solar wind and corona [32], as well as the suppression of turbulent transport in laboratory plasmas [29, 33, 34].

This work was supported by NSF grants ATM-0852682 and ATM-0646442 and NASA grant NNX10AK97G to Auburn University, grants NSFC 41028003 and NSFC 40890163, and at PPPL by NASA grants (NNG07EK69I, NNH07AF37I, NNH09AM53I, NNH09AK63I, and NNH11AR07I), NSF grant ATM0902730, and DOE contract DE-AC02-09CH11466. Computer resources were provided by NAS and ASC.

---

* ylin@physics.auburn.edu

[1] T. H. Stix, *Waves in Plasmas* (New York: American Institute of Physics, 1992).

[2] A. Hasegawa and K. Mima, J. Geophys. Res. **83**, 1117 (1978).

[3] L. C. Lee, J. R. Johnson, and Z. W. Ma, J. Geophys. Res. **99**, 17405.

[4] J. R. Johnson and C. Z. Cheng, Geophys. Res. Lett. **24**, 1423 (1997).

[5] L. Chen, J. Geophys. Res. **104**, 2421 (1999).

[6] Y. Song and R. L. Lysak, Space Sci. Rev. **95**, 273 (2001).

[7] C. Chaston, J. Bonnell, J. P. McFadden, C. W. Carlson, C. Cully, O. Le Contel, A. Roux, H. U. Auster, K. H. Glassmeier, V. Angelopoulos, and C. T. Russell, Geophys. Res. Lett. **351**, L17S08 (2008).

[8] W. Lotko, A. V. Streltsov, and C. W. Carlson, Geophys. Res. Lett. **25**, 4449 (1998).

[9] M. Tanaka, T. Sato, and A. Hasegawa, Phys. Fluids B **1**, 325 (1989).

[10] B. D. G. Chandran, Astrophys. J. **720**, 548 (2010), arXiv:1006.3473 [astro-ph.SR].

[11] S. W. McIntosh, B. de Pontieu, M. Carlsson, V. Hansteen, P. Boerner, and M. Goossens, Nature **475**, 477 (2011).

[12] R. R. Mett and S. M. Mahajan, Phys. Fluids B **4**, 2885 (1992).

[13] K. L. Wong, N. Bretz, G. Y. Fu, J. Machuzak, J. R. Wilson, Z. Chang, L. Chen, D. K. Owens, and G. Schilling, Phys. Lett. A **224**, 99 (1996).

[14] A. Fasoli, J. B. Lister, S. Sharapov, D. Borba, N. Deliyanakis, C. Gormezano, J. Jacquinot, A. Jaun, H. A. Holties, G. T. A. Huysmans, W. Kerner, J.-M. Moret, and L. Villard, Phys. Rev. Lett. **76**, 1067 (1996).

[15] M. M. Hoppe and C. T. Russell, J. Geophys. Res. **88**, 2021 (1983).

[16] Y. Lin, J. R. Johnson, and X. Y. Wang, J. Geophys. Res. **115**, A04208 (2010).

[17] T. Tamao, Sci. Rep. Tohoku Univ., Ser. 5, Geophys. **17**, 43 (1965).

[18] C. Uberoi, Phys. Fluids **15**, 1673 (1972).

[19] L. Chen and A. Hasegawa, Phys. Fluids **17**, 1399 (1974).

[20] D. J. Southwood, Planet. Space Sci. **22**, 483 (1974).

[21] A. Hasegawa and L. Chen, Phys. Fluids **19**, 1924 (1976).

[22] J. R. Johnson, C. Z. Cheng, and P. Song, Geophys. Res. Lett. **28**, 227 (2001).

[23] A. Hasegawa and L. Chen, Physical Review Letters **36**, 1362 (1976).

[24] A. Frieman and L. Chen, Phys. Fluids **25**, 502 (1982).

[25] L. Chen and F. Zonca, EPL **36**, 35001 (2011).

[26] L. Chen, Z. Lin, R. B. White, and F. Zonca, Nuc Fusion **41**, 747 (2001).

[27] O. G. Onishchenko, O. A. Pokhotelov, R. Z. Sagdeev, L. Stenflo, R. A. Treumann, and M. A. Balikhin, J. Geophys. Res. **109**, A03306 (2004).

[28] J. S. Zhao, D. J. Wu, J. Y. Lu, YangL., and M. Y. Yu, New J. Phys. **13**, 063043 (2011).

[29] Z. Lin, T. S. Hahm, W. W. Lee, W. M. Tang, and R. B. White, Science **281**, 1835 (1998).

[30] C. C. Chaston, J. R. Johnson, M. Wilber, M. Acuna, M. L. Goldstein, and H. Reme, Physical Review Letters **102**, 015001 (2009).

[31] O. A. Pokhotelov, O. G. Onishchenko, R. Z. Segdeev, and R. A. Treumann, J. Geophys. Res. **108**, 1291 (2003).

[32] S. R. Cranmer and A. A. van Ballegooijen, Astrophys. J. **594**, 573 (2003), arXiv:astro-ph/0305134.

[33] P. H. Diamond, S.-I. Itoh, K. Itoh, and T. S. Hahm, Plasma Physics and Controlled Fusion **47**, 35 (2005).

[34] W. X. Wang, T. S. Hahm, W. W. Lee, G. Rewoldt, J. Manickam, and W. M. Tang, Physics of Plasmas **14**, 072306 (2007).